Future trends of global agricultural emissions of ammonia in a changing climate

M Beaudor[1,2], N Vuichard[1], J Lathière[1], D Hauglustaine[1]

[1]Laboratoire des Sciences du Climat et de l'Environnement (LSCE) CEA-CNRS-UVSQ, Gif-sur-Yvette, France

[2]The High Meadows Environmental Institute, Princeton University, Princeton, NJ, USA

Key Points:

- Development of downscaling method to project global gridded livestock densities and ammonia emissions from agriculture until 2100
- Global future ammonia emissions in 2100 range up to 70 TgN.yr^{-1} depending on the scenario representing an increase of 30 to 50 % compared to present-day
- Climate change is estimated to contribute up to 20% of the increase in total emission

Corresponding author: Maureen Beaudor, `mb0142@princeton.edu`

Abstract

Because of human population growth, global livestock, and associated ammonia, emissions are projected to increase through the end of the century, with possible impacts on atmospheric chemistry and climate. In this study, we propose a methodology to project global gridded livestock densities and NH_3 emissions from agriculture until 2100. Based on future regional livestock production and constrained by grassland distribution evolution, future livestock distribution has been projected for three Shared Socio-economic Pathways (SSP2-4.5, SSP4-3.4, and SSP5-8.5) and used in the CAMEO process-based model to estimate the resulting NH_3 emissions until 2100. Our global future emissions compare well with the range estimated in Phase 6 of the Coupled Model Intercomparison Project (CMIP6), but some significant differences arise within the SSPs. Our global future ammonia emissions in 2100 range from 50 to 70 $TgN.yr^{-1}$ depending on the SSPs, representing an increase of 30 to 50 % compared to present day. Africa is identified as the region with the most significant regional emission budget worldwide, ranging from 10 to 16 $TgN.yr^{-1}$ in 2100. Through a set of simulations, we quantified the impact of climate change on future NH_3 emissions. Climate change is estimated to contribute to the emission increase of up to 20%. The produced datasets of future NH_3 emissions is an alternative option to IAM-based emissions for studies aiming at projecting the evolution of atmospheric chemistry and its impact on climate.

Plain Language Summary

Due to the growing global population and increased livestock farming, emissions of ammonia (NH_3) are expected to rise until the end of the century with possible impacts on air quality and climate. This study introduces a method to predict livestock densities and NH_3 emissions worldwide until 2100. We estimate future livestock distribution based on different socio-economic scenarios and used a modeling approach to quantify resulting NH_3 emissions. The predicted global NH_3 emissions align well with estimates from a major climate modeling project, but there are variations within the scenarios studied. By 2100, global ammonia emissions may increase by 30 to 50%, reaching 50 to 70 $TgN.yr^{-1}$, with Africa becoming one of the most important emitter regions. Due to their sensitivity to environmental conditions, NH_3 emissions are expected to be enhanced by climate change whose contribution can reach 20%. The data generated in this study provides an alternative to traditional emissions projections which usually overlook climate sensitivity. This aims to help for a better understanding of future air pollution and its interactions with climate.

1 Introduction

Global NH_3 emissions rose from 55 to 65 $TgN.yr^{-1}$ between 2000 and 2015, mainly caused by the increasing livestock production and fertilizer use (van Marle et al., 2017; Hoesly et al., 2018). Livestock production is inextricably linked to land-use and land-management to support animal feed needs. Land dedicated to feed production represents the most significant land-use system present-day, occupying up to 45 % of the global land area (Reid et al., 2008). The global consumption of meat increased by 35 % over the last 25 years (Herrero et al., 2009). This evolution was accompanied by the development of livestock production systems in many countries with important consequences on land-use. For instance, due to the expansion of cattle ranching, forests are cleared to establish new pastures along with frequent arable land expansions such as soybean cultivation in Brazil (Barona et al., 2010). In the future, the African agricultural sector will most likely also experience a crucial evolution with, for instance, an estimated 10-time increase in livestock production by the end of the century under a high development rate scenario (Riahi et al., 2017).

While emissions of some species such as SO_2 and NO_x are expected to be down-regulated in the future, NH_3 emissions, which mainly originate from the agricultural sector, are projected to increase under all the Shared Socio-economic Pathways (SSPs) for the 21st century (Paulot et al., 2016). Recent atmospheric modeling studies have shown the key role of future NH_3 emissions in the formation of ammonium nitrate aerosols and their effect on the radiative forcing (Hauglustaine et al., 2014; Bian et al., 2017; Pai et al., 2021). Because of the impact of NH_3 on air quality and climate, it is of high interest to understand how the evolution of the agricultural sector could drive future emissions under different SSPs and climate scenarios. In the framework of Phase 6 of the Coupled Model Intercomparison Project (CMIP6), ScenarioMIP (O'Neill et al., 2016; Riahi et al., 2017) provides scenarios of future evolution for the main drivers impacting the climate system and under the different SSPs. In this context, NH_3 emission projections have been produced by Integrated Assessment Models (IAMs) which consist of simplified but consistent representations of the socio-economy, land systems, and their interactions. These emission projections are the data that have been used for the atmospheric chemistry component of ESMs involved in AerChemMip (Collins et al., 2017). While this effort constitutes so far the only existing emission projections for the future, it is worth noting that it has several limitations. A harmonization and downscaling of IAM's future emissions have been developed (Gidden et al., 2018) to be consistent with historical emissions and to move from the IAM original regional scale (around ten regions at global scale depending on the IAM) to gridded data. The downscaling methodology applied assumes that the spatial pattern within each large region is kept constant over time using the information from the end of the CMIP6 historical period (ie 2014). In addition, this harmonization and downscaling procedure has only been applied to one IAM for each SSP. The approaches used for modeling emissions in the IAMs are significantly different, which makes the set of projected emissions for the different SSPs inconsistent. Last, future ammonia emissions projected by IAMs do not account for the impact of climate and environmental change, while they are important drivers of emissions.

In this paper, we estimate the agricultural ammonia emissions over 2015-2100 for three SSPs using the single process-based model named Calculation of AMmonia Emissions in ORCHIDEE (CAMEO, Beaudor et al., 2023). Driven by projections of gridded livestock densities and pasture area at a fine scale, the spatial pattern of the projected ammonia emissions is evolving over the 21st century where pasture expands. In Section 2, we describe the method used to construct future livestock density and the set of experiments developed within this study to estimate NH_3 emissions. Section 3 presents the future livestock densities along with agricultural NH_3 emissions and a comparison of the trends with NH_3 emission projections performed by IAMs in the CMIP6 context. We also include an assessment of the key drivers that might impact future emissions and, in particular, the contribution of climate change. Finally, a global and regional analysis of the emissions in 2100 is presented.

2 Methods

2.1 The CAMEO model

Future emissions are calculated by the process-based model CAMEO (see Beaudor et al., 2023) for a detailed description of the model along with an evaluation). The model simulates the manure production and agricultural NH_3 emissions from the manure management chain (including manure storage and grazing) and soil emissions due mostly to synthetic fertilizer and manure applications. CAMEO is integrated into the global Land Surface Model ORCHIDEE (Krinner et al., 2005; Vuichard et al., 2019). ORCHIDEE is constrained by meteorological fields, land-use maps, and N input such as synthetic fertilizers. CAMEO has been extensively evaluated for the present-day in Beaudor et al. (2023) showing a good agreement of intermediate variables with recent literature results (i.e. global crop and grass production, biomass dedicated to livestock, manure

production, fertilization application, and agricultural ammonia emissions). Within this last study, multiple sensitivity tests have also been conducted to evaluate the response of CAMEO to internal parameters (i.e. soil pH, indoor emission factors, the timing of fertilization, and atmospheric concentration). To complete this evaluation, the authors have compared the seasonality of CAMEO emissions to satellite-derived emissions (method described in Evangeliou et al., 2020) and other modeling/inventory datasets highlighting very satisfying correlation scores. As the forcing files used in this study are not exactly the same as used in the reference study from Beaudor et al. (2023), an additional analysis is provided in the Supplementary Material (Figure S1) to ensure that the seasonal patterns of the model are conserved against IASI-derived emissions. In fact, using the CMIP6 forcing files (described hereafter) improve the seasonal variability in the US and China where the original emissions were likely too high during July and might be explained by higher synthetic fertilizer input or enhancement from meteorology conditions.

Livestock densities represent one of the most critical input for CAMEO since it is the main driver of the feed need estimation and, thus, of indoor and -to a lesser extent -soil emissions. In CAMEO, estimated livestock densities, actually considered, can be lower than prescribed ones under specific conditions where biomass resources are limited, as diagnosed by the ORCHIDEE model. Indeed, they assume that the grass feed requirement at the grid cell level is satisfied locally and with no grass import. To account for this limitation, CAMEO computes a grazing indicator (GI) which corresponds to the fraction of grass NPP for the year y that is exported and used for the ruminant needs. The GI maximum value is set at 0.7, defined as the maximum of the above-ground biomass available for grazing/cutting.

2.2 CAMEO forcings for 2015-2100

- Meteorology :
  To drive CAMEO/ORCHIDEE, we used 3-hourly near-surface meteorological fields simulated by the IPSL-CM6A-LR Earth System Model (Boucher et al., 2020) in the context of CMIP6 for near-surface air temperature, specific humidity, wind speed, pressure, short- and longwave incoming radiation, rainfall, and snowfall. We used the HIST experiment outputs for the present-day conditions and those produced within ScenarioMIP (O'Neill et al., 2016) for the future climate. For both historical and future simulations, we used the r1i1p1f1 member of each experiment.
- Land-use:
  Data used in this study originate from the Land Use Harmonization -2 dataset developed in the framework of CMIP6 (LUH2, Hurtt et al., 2020). It provides land-use reconstruction over the period 1850-2014 for key aggregated land categories (primary lands, secondary lands, pasture, croplands, etc..). and land-use projections over 2015-2100 for the different SSPs used in CMIP6. The SSPs allow the consideration of a wide range of mitigation efforts on emissions. Each pathway corresponds to a specific scenario designed by an IAM where the emissions are a function of a complex interaction between socio-economic factors (Riahi et al., 2017). The procedure to translate LUH2 land categories in ORCHIDEE plant functional types is described in Lurton et al. (2020).
- N input:
  Information on the mineral fertilizer applied on C3 and C4 type cropland is part of the LUH2 dataset (Hurtt et al., 2020). NH_x and NO_y depositions fields have been produced by CAM-Chem model in the framework of CMIP6 and are available on input4MIP from 2015 to 2100 (Hegglin et al., 2016, n.d.).
- Livestock density:
  The present-day livestock density is defined by the Gridded Livestock of the World (GLW 2, Robinson et al., 2014). It provides livestock information at a quarter de-

167 gree for the main livestock categories (cattle, sheep, goat, pig, and poultry). Data
168 is available for 2006 only, which is used and kept constant for every year of the
169 HIST simulation. To our knowledge, there is no gridded product similar to GLW2
170 for future scenarios over 2015-2100. The IIASA database
171 (https://tntcat.iiasa.ac.at/SspDb/dsd?Action=htmlpage&page=about) pro-
172 vides livestock production projections ($L_{SSP,reg,dec}$, million tDM/yr, see Figure S2
173 in the Supplementary Material) over the period 2010-2100 per decade (dec) for
174 all the SSPs described in Riahi et al. (2017), but only for five large regions (reg)
175 over the globe (Asia, Latin America, Africa, OECD countries, Reforming Economies
176 of Eastern Europe countries). The following section describes the methodology
177 developed to reconstruct the future gridded livestock densities.

2.3 Downscaling methodology for future livestock densities

179 For each livestock category, we constructed the future gridded livestock density for
180 a given SSP ($D_{l,SSP}$, heads.m^{-2}) based on the historical livestock density from GLW2
181 ($D_{l,GLW2}$), and the livestock production evolution assessed by the SSP-related IAM for
182 2010-2100 for the five large regions defined by IIASA ($L_{SSP,reg,dec}$). The IIASA database
183 provides only information for total livestock and not for specific livestock categories. As
184 a consequence, we assumed that the relative distribution of the livestock categories is
185 kept constant over time, at the regional scale but also within the grid cells, using the GLW2
186 information for the present-day.

187 The general aim is to reflect the future livestock production at the regional scale
188 by varying their local spatial pattern within each region according to the future evolu-
189 tion of grassland areas. To first respect the future livestock production change at the re-
190 gional scale projected by the IAMs, we need to satisfy the following equation:

$$\frac{D_{l,SSP,dec,reg}}{D_{l,GLW2,reg}} = \frac{L_{SSP,reg,dec}}{L_{SSP,reg,2010}} \quad (1)$$

191 where $D_{l,GLW2,reg}$ and $D_{l,SSP,dec,reg}$ are the regional-mean values for the region reg of re-
192 spectively $D_{l,GLW2}$ and $D_{l,SSP}$ for the decade dec and $L_{SSP,reg,2010}$, the value of $L_{SSP,reg,dec}$
193 for 2010. We note $f_{SSP,reg,dec}$ the ratio $\frac{L_{SSP,reg,dec}}{L_{SSP,reg,2010}}$.

194 In our modeling framework, we did the assumption that grass-feed livestock needs
195 (BM_{grass}, gC.m^{-2}.yr^{-1}) were locally produced (within the grid cell) (Beaudor et al., 2023).
196 BM_{grass} is computed as:

$$BM_{grass} = aNPP_{grass} \times f_{grass} \times GI \quad (2)$$

197 where $aNPP_{grass}$ is the above-ground Net Primary Productivity of grassland (gC.m$^{-2}_{[grass]}$.yr^{-1}),
198 f_{grass}, the fraction of grassland in the grid cell and GI a parameter named Grazing In-
199 tensity (unitless) which corresponds to the fraction of NPP "exported" for animal feed-
200 ing (see Beaudor et al., (Beaudor et al., 2023)). The grass feed produced locally in a grid
201 cell may increase or decrease for the different SSPs, as does f_{grass} in LUH2, which en-
202 ables to sustain a variable livestock production over time. Because we want to account
203 for this "extensification" term, we do not apply directly the $f_{SSP,reg,dec}$ factor to the live-
204 stock density in a given grid cell "c", $D_{l,GLW2,c}$, to get $D_{l,SSP,dec,c}$. Instead, we computed
205 a variable $f_{SSP,c,dec}$ for each grid cell based on the ratio between the grass feed produced
206 in the grid cell c in future decade 'dec' ($BM_{grass,SSP,c,dec}$) and in the year 2010 ($BM_{grass,c,2010}$):

$$f_{SSP,c,dec} = \frac{BM_{grass,SSP,c,dec}}{BM_{grass,c,2010}} \quad (3)$$

208 As a simplification, we assumed that grassland productivity will not be impacted by cli-
209 mate change and will remain constant at its 2010 value for any SSP. In addition, we did
210 assume that the grazing intensity will be a fraction of its 2010 value, fixed at the regional
211 level ($x_{SPP,reg,dec}$). However, as done in Beaudor et al. (2023), we limited the GI to 70%

of the above-ground NPP (0.7). As a consequence, $f_{SSP,c,dec}$ may be written as:

$$f_{SSP,c,dec} = \frac{aNPP_{grass,c,2010} \times f_{grass,SSP,c,dec} \times \min(0.7, GI_{c,2010} \times x_{SPP,reg,dec})}{aNPP_{grass,c,2010} \times f_{grass,c,2010} \times GI_{c,2010}} \quad (4)$$

$f_{grass,c,2010}$ and $f_{grass,SSP,c,dec}$ are the fractions of grassland in the grid-cell c for respectively 2010 and decade 'dec' taken from LUH2 (Hurtt et al., 2020) (see more details in the "Land-use data" in Section 2.2). $x_{SPP,reg,dec}$ is the single unknown of Eq. 4 which is set by satisfying the following equation:

$$f_{SSP,reg,dec} = \frac{\sum_{c=1}^{n_{reg}} BM_{grass,SSP,c,dec} \times Areas_c}{\sum_{c=1}^{n_{reg}} BM_{grass,c,2010} \times Areas_c} \quad (5)$$

where n_{reg} is the number of grid cells within the region reg and $Areas_c$ the area of the grid cell c.

The final step consists in multiplying the resulting $f_{SSP,c,dec}$ (depicted in Figure S3 in Supplementary Material) to the historical total livestock density ($D_{l,GLW2}$) and retrieving the future livestock density per animal category based on the historical proportion of animal category at each grid-cell. Once each decade is reconstructed, a linear interpolation is applied to retrieve the intermediate year. From 2011 to 2019, we use as initial and final interpolation points the reference distribution for 2010 and the corresponding SSP distribution of the decade 2020.

2.4 Simulations set-up

The ORCHIDEE model, including CAMEO, was run at the spatial resolution of the IPSL-CM6A-LR Earth System model (2.5° lon x 1.27° lat). We first performed a 15-year historical simulation over the 2000-2014 period (called HIST) using the meteorological near-surface fields from the CMIP6 HIST experiment of IPSL-CM6A-LR (Boucher et al., 2019). In the HIST simulation, all forcing data are updated yearly, except those related to livestock density, which is kept constant over time (GLW, Robinson et al., 2014).

A set of 3 future scenarios was conducted to evaluate the impact of future changes in agricultural practices (livestock densities and use of fertilizers) on agricultural ammonia emissions.

Among the SSPs developed within ScenarioMip, we used the three SSPs that correspond to the most divergent trajectories of livestock production: SSP2-4.5 (Middle of the Road, Fricko et al., 2017), SSP4-3.4 (A world of deepening inequality, Calvin et al., 2017) and SSP5-8.5 (Fossil-fueled Development – Taking the Highway, Kriegler et al., 2017). SSP4-3.4 is the scenario with the weakest livestock evolution, while SSP5-8.5 is the one with the biggest increase. SSP2-45 shows an intermediate evolution between SSP4-3.4 and SSP5-8.5 (Figure S2 in the Supplementary Material). These three scenarios are also divergent in terms of agricultural productivity and human population evolution, food demands and dietary preferences. For instance, SSP5-8.5 presents a world characterized by meat-rich diets and important waste while SSP2-4.5 reflects medium animal demand and SSP4-3.4 presents important regional differences with high consumption lifestyles in elite socio-economic categories and low consumption for the rest (Popp et al., 2017).

In order to assess the sensitivity of the emissions to future climate change, the three scenarios were repeated under two types of climate (historical and future). The SSP simulations under a future climate are called 'SSP$_i$' (with i: 2-4.5, 4-3.4 or 5-8.5). They account for all SSP-related forcings and are driven by the climate data simulated by the IPSL-CM6 model for each SSP scenario. These simulations are considered as reference simulations. Other simulations are driven by cyclic historical climatology (2011-2014) for the meteorology and a fixed value for [CO_2] corresponding to the year 2014 are labeled "SSP$_i$Clim$_{HIST}$". The 'SSP$_i$' and "SSP$_i$Clim$_{HIST}$" simulations were run for 86 years over the 2015-2100 period starting from the last year of the HIST simulation. All forc-

Table 1. Summary of the simulations performed with the corresponding forcing files. A unique [CO_2] value is shown in the table to provide a comparison point between the simulations.

Run name (Run period)	Meteo[a]	[CO_2][b]	Land cover, Fertilizer[c]	Nitrogen deposition[d]	Livestock[e]
HIST (2002-2014)	$HIST_y$	$[CO_2]_{2014}^{2002} = 385$	UofMD-landState	HIST	REF
$SSP_{2-4.5}$ (2015-2100)	ssp2-4.5	$[CO_2]_{2100}^{2015} = 502$	MESSAGE-ssp2-4.5	ssp2-4.5	ssp2-4.5
$SSP_{4-3.4}$ (2015-2100)	ssp4-3.4	$[CO_2]_{2100}^{2015} = 437$	GCCAM4-ssp4-3.4	ssp4-3.4	ssp4-3.4
$SSP_{5-8.5}$ (2015-2100)	ssp5-8.5	$[CO_2]_{2100}^{2015} = 768$	MAGPIE-ssp5-8.5	ssp5-8.5	ssp5-8.5
$SSP_{2-4.5}-$ $Clim_{HIST}$ (2015-2100)	$HIST_{clim}$	$[CO_2]_{2014} = 398$	MESSAGE-ssp2-4.5	ssp2-4.5	ssp2-4.5
$SSP_{4-3.4}-$ $Clim_{HIST}$ (2015-2100)	$HIST_{clim}$	$[CO_2]_{2014} = 398$	GCCAM4-ssp4-3.4	ssp4-3.4	ssp4-3.4
$SSP_{5-8.5}-$ $Clim_{HIST}$ (2015-2100)	$HIST_{clim}$	$[CO_2]_{2014} = 398$	MAGPIE-ssp5-8.5	ssp5-8.5	ssp5-8.5

a Taken from IPSL-CM6A-LR Earth System Model (see details in Section 2.2); $HIST_y$: y correspond to a yearly meteorological field while $HIST_{clim}$ is a cycling over 2011-2014.

b units in ppm. $[CO_2]_{yf}^{yi}$ represents the mean value between years yi and yf, but note that the simulation uses an annual mean value; in the 'Clim$_{HIST}$' simulations, a fixed value corresponding to year 2014 is taken ($[CO_2]_{2014}$).

c LUH2 version 2.1h for HIST and version 2.1f for SSPs.

d input4MIPs.CMIP6.CMIP.NCAR.NCAR-CCMI-v1-0 for HIST and v2-0 for SSPs

e Livestock distributions for SSPi correspond to the reconstructed projected livestock distribution dataset ($DISTR_{SSPi}$) described in Section 2.3.

ing data were updated every year, including the livestock distributions in this set of simulations. The different simulations and their corresponding forcing files are summarized in Table 1 and described in the following section.

2.5 Comparison against future IAM-based emissions

We compared the simulated agricultural NH_3 emissions, to those produced by the Integrated Assessment Models (IAMs) in the context of input4MIPs (Gidden et al., 2018) for the three SSPs considered in this study. The IAMs developed specific methods for estimating NH_3 emissions with characteristics regarding agricultural NH_3 emissions listed in Table 2. Different IAMs estimate agricultural NH_3 emissions for the three SSPs considered in this study. Emission calculation in any of the IAMs is based on regional emission factors (EFs) applied to specific activity input levels (livestock, crop, or managed grassland input). While MESSAGE-GLOBIOM model uses its own EFs, GCAM and REMIND-MAgPIE models are based on reference EFs from the EDGAR inventory (Janssens-Maenhout, 2011), or the IPCC methodology (Paustian et al., 2006). Emission estimation from REMIND-

Table 2. Method and input tables used within the three IAMs to develop agricultural NH_3 emission estimates in the framework of the SSPs. EF account for regional emission factor applied to the specified activity level (livestock, crop or grass input). Grass input corresponds to managed grassland. According to Rao et al. (2017).

IAM	*SSP*	*Livestock input* (EF sources)	*Crop input* (EF sources)	*Grass input* (EF sources)
MESSAGE-GLOBIOM	*2-4.5*	Livestock production (GLOBIOM)	Crop production (GLOBIOM)	–
GCCAM	*4-3.4*	Livestock production (Edgar 4.2)	Crop production (Edgar 4.2)	–
REMIND-MAgPIE	*5-8.5*	Nr. of animals, feed (MAgPIE/ IPCC 1996, 2006)	Cropland soil : Fertilizer, manure, other N inputs (MAgPIE / IPCC 2006)	N manure input (MAgPIE / IPCC 2006)

MAgPIE IAM is the most complex and realistic approach considering manure application over managed grasslands.

3 Results

3.1 Evolution of livestock distribution until 2100

As a preliminary result, we show the evolution of the resulting regional factor $f_{\text{SSP,reg,dec}}$ from 2020 to 2100, along with the theoretical target representing the change in livestock production (Figure 1). In all regions, except Africa and Latin America, the target is nearly reached for all three scenarios, meaning that the projected livestock can be satisfied by the regional modelled biomass. In Africa and Latin America, the target is far from being reached, especially under SSP5-8.5 in Africa from 2030. In 2100, the target is three times higher than what is possible to sustain with the future grassland area and the maximal use of grass NPP.

The resulting reconstructed maps for decades 2020, 2030, 2050, and 2100 of the livestock distributions simulated by CAMEO are depicted in Figure S4 in Supplementary Material. The regions with the most significant increase in total livestock in 2100 are central and South Africa and eastern Asia under SSP4-3.4 and SSP5-8.5. In Africa, where densities were rather around 200 Heads.$\text{km}^{-2}.\text{yr}^{-1}$ in 2000, the livestock can reach 8000 Heads.$\text{km}^{-2}.\text{yr}^{-1}$ in 2100. Even earlier (in 2030), Africa is the region where livestock experiences the most significant increase (historical density $\times$ 40, see Figure S3 in the Supplementary Material). It is worth noting that some critical differences in the gridded factors $f_{\text{SSP,c,dec}}$ can exist spatially within one region depending on the present-day value of GI and the evolution of the pasture lands (see Figure S3 in the Supplementary Material).
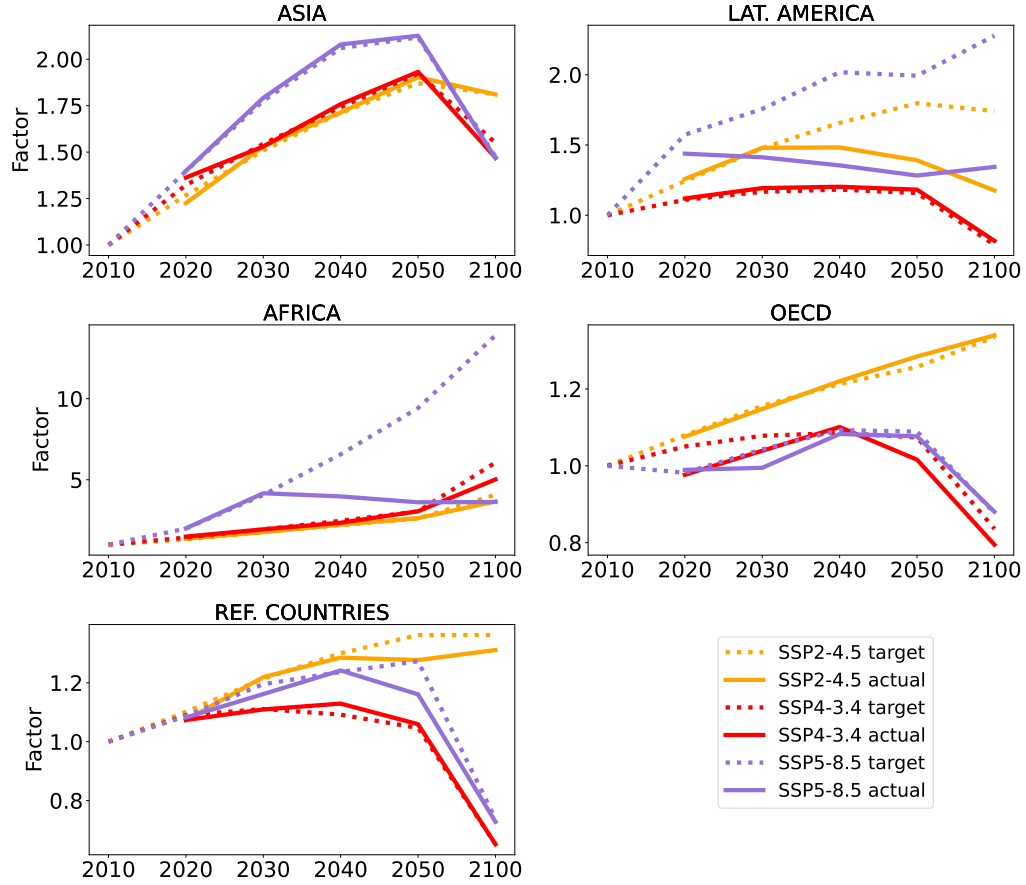
Figure 1. Regional factors $f_{SSP,reg,dec}$ for three different SSPs (plain lines). The dotted lines represent the target without biomass productivity constraints. The regional abbreviation 'REF' accounts for the Reforming Economies of Eastern Europe and the Former Soviet Union. Please note the different y-axis ranges for the different regions.

3.2 Future trends of ammonia emissions under climate change and comparison with the IAM's estimates

The evolution of the emissions under the three SSPs simulated by CAMEO ranges between 35-70 TgN.yr^{-1} (Figure 2) This estimate is close to the one estimated by IAMs (Riahi et al., 2017) in 2100 (38-65 TgN.yr^{-1}, Figure 2). The global evolution of the agricultural emissions simulated by CAMEO shows an increase of around 50% by 2100 compared to 2014 under the SSP4-3.4 and SSP2-4.5, which have similar trends. Under the SSP5-8.5, the evolution is more steady and reaches its maximum value in 2040 (32%). CAMEO emission trends are close to IAM projections for SSP4-3.4 and SSP5-8.5 even though CAMEO emissions do not decrease after 2080 as in IAMs. Moreover, there is an important difference between CAMEO and IAMs under the SSP2-4.5, where CAMEO emissions surpass the IAMs estimations by 25 TgN.yr^{-1}, with opposite trends. In our approach, SSP2-4.5 highlights the most crucial increase, while for IAMs, SSP2-4.5 is the "weakest" scenario (in 2100, emissions reach the same value as in the present day). Analyzing the relationship between NH$_3$ emissions and livestock production simulated by the different IAMs specifically for the SSP2-4.5 indicates that in the MESSAGE-GLOBIOM model (the reference IAM for the marker scenario SSP2-4.5) both variables are poorly

and negatively correlated which is contrary to the other IAMs (Figure S5 in the Supplementary Material). In addition, MESSAGE-GLOBIOM is the model that simulates the lowest emission rate over 2080-2100 (34 % lower than the IAM average) not only for SSP2-4.5 but also for other SSPs (not shown here).
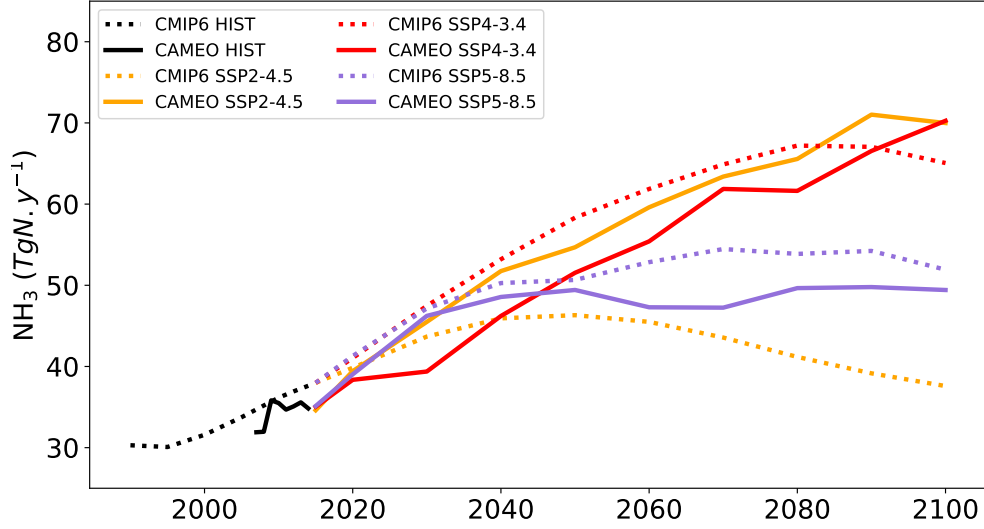

Figure 2. Evolution of the global agricultural NH_3 emissions for the considered SSPs from CAMEO under future climate (solid lines) and from the CMIP6 inventory (dotted lines from IAMs, Gidden et al., 2018), in $TgN.yr^{-1}$.

Regional trends of NH_3 emissions and N input for the biggest emission regions are shown in Figure 3 and Figure 4. It is important to note that the information about fertilizer inputs used in CAMEO is the one provided by IAMs (through the LUH2 dataset), while other N inputs but also the way ammonia emissions are computed, are different between CAMEO and IAMs. Even though CAMEO and IAMs emissions are well correlated for the SSP5-8.5 at the global scale, their trends vary significantly at the regional scale. For instance, in Africa, the simulated CAMEO emissions reach a plateau of around 10 $TgN.yr^{-1}$ in 2030, while IAMs emissions show a positive trend until 2080, reaching a maximum value of 20 $TgN.yr^{-1}$. In this region, manure application rates simulated by CAMEO also reached a plateau as the fertilizer application rates a few decades later (Figure 4). Due to the high increase in manure production over the first decades and its importance in the total N input (around 65%), livestock distribution likely plays a crucial role (compared to the fertilizer application) in the resulting emission trend.

The differences in total emissions under SSP2-4.5 are also significant at the regional scale. In all the regions, the CAMEO emissions exceed the emissions estimated by the IAM, except in India (Figure 3). In Europe, Latin America, and Africa, the fertilizer input under SSP2-4.5 is at its highest with at least 10 $TgN.yr^{-1}$ of differences compared to the other SSPs over the 2030-2100 period (Figure 4). Combined with a similar pattern in manure production, mainly due to a constant increase in livestock production, it partly explains why SSP2-4.5 is distinguishable from the other SSPs in our approach. In the IAMs, even though the emissions are also the highest under SSP2-4.5 in Europe and Latin America, we mainly observe steady or negative trends in China, Latin America, Africa, and the US, which explains the global decreasing trend. These results in emissions in Latin America, Africa, and the US are contrary to the fertilizer input trends showed
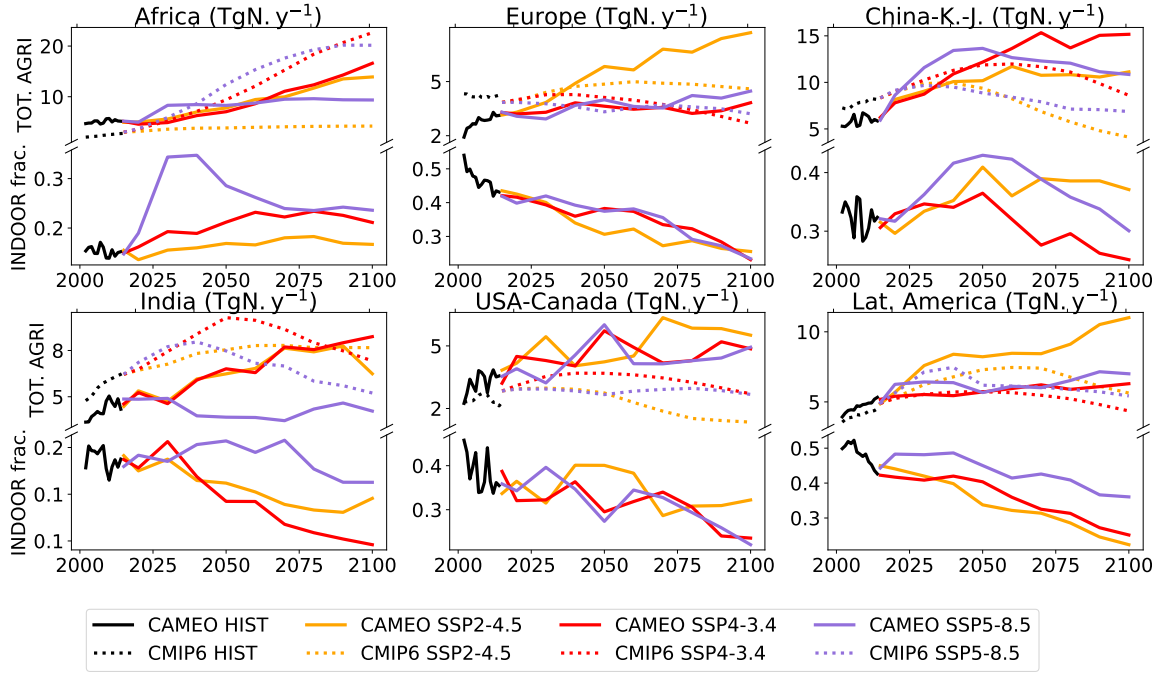
Figure 3. Evolution of the regional NH_3 emissions for the considered SSPs from the agricultural sector and the fraction of indoor manure management simulated by CAMEO (solid lines) and total agricultural from the CMIP6 inventory (IAMs Gidden et al. (2018), dotted lines) in $TgN.yr^{-1}$.

in Figure 4. Contrary to the IAMs, while the fertilizer input appears to play a minor role in the temporal evolution, our approach seems to better capture the trends. In China, for instance, the total agricultural input is particularly high under SSP4-3.4 with 30 $TgN.yr^{-1}$ more than under other SSPs in 2100 (explained mainly by the fertilizer application). Despite this critical difference, the resulting total emissions do not highlight specifically much higher emissions than the other SSPs.

Not considering climate change as a driver of ammonia emissions is another limitation of the IAM methodology. Indeed, with CAMEO, we estimated a non-negligible contribution of climate change in the future emissions which reaches 7 % to 22 % by 2100, for SSP2-4.5 and SSP5-8.5, respectively (Table 3). Change in emissions with temperature and precipitation under SSP5-8.5 differs significantly from the two other scenarios at the end of the century (Figure S6 in the Supplementary Material) where the meteorological conditions are extreme (temperature and rain range up to +7.5 K and +0.5 mm/day respectively over 2080-2100). The sensitivity of the emissions to these two meteorological variables depends on the scenario. For instance, under SSP5-8.5, agricultural emissions are simulated to increase by 3 % / K and by 14 %/mm/day. As expected, the evolution of the total agricultural emissions under climate change is well correlated to the change in soil ammonium content, an important proxy for soil emissions. On another hand, indoor emissions in CAMEO are only indirectly dependent on the climate mainly through the managed NPP (as feed for livestock), a variable much less sensitive to climate (by 0.22 % / K and by 3.6 %/ mm/day, Figure S6 in the Supplementary Material). We might also expect a role of CO_2 increase in the emission change especially under SSP5-8.5 (not studied here). In almost all regions, we observe the biggest changes in the emis-
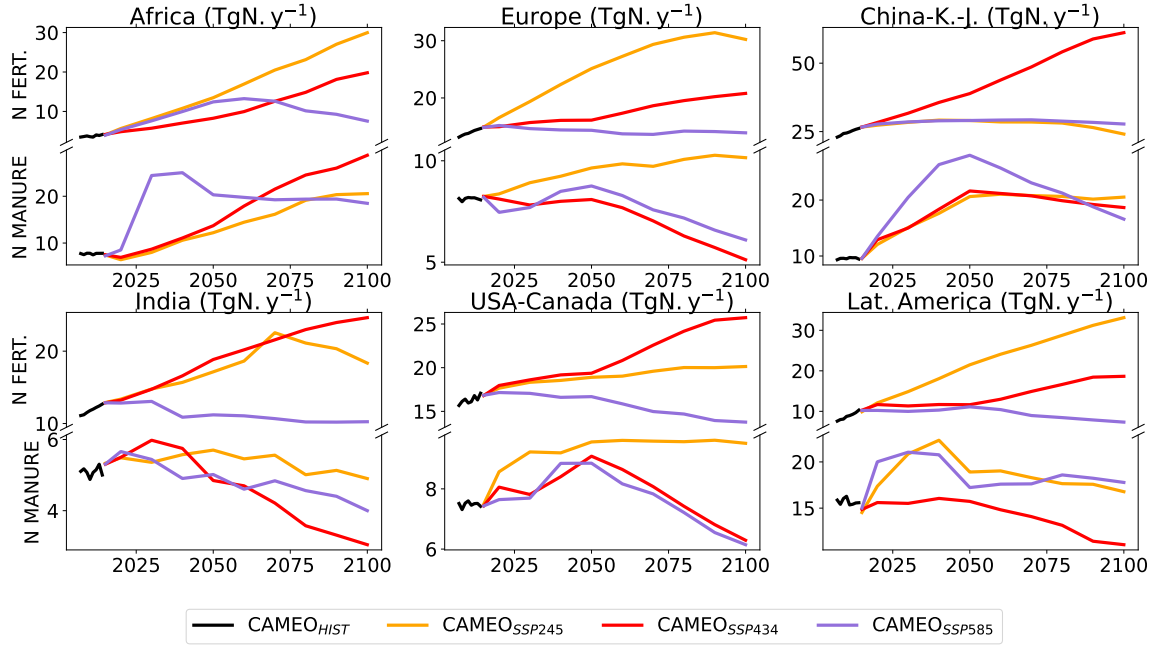
Figure 4. Evolution of the regional N input for the considered SSPs including the manure production simulated by CAMEO and the mineral fertilizer use from CMIP6 in TgN.yr^{-1}.

sions due to climate under SSP5-8.5, especially during the last decades of the century (Figure 5). In Asia, climate change has also a strong positive impact on emissions under SSP4-3.4 (1 to 2.5 TgN.yr^{-1}).

Table 3. Global agricultural NH$_3$ emissions (TgN.yr^{-1}) for the historical period (2005-2014) and under different SSPs over 2091-2100 simulated by CAMEO under future and historical climate and estimated by the IAMs.

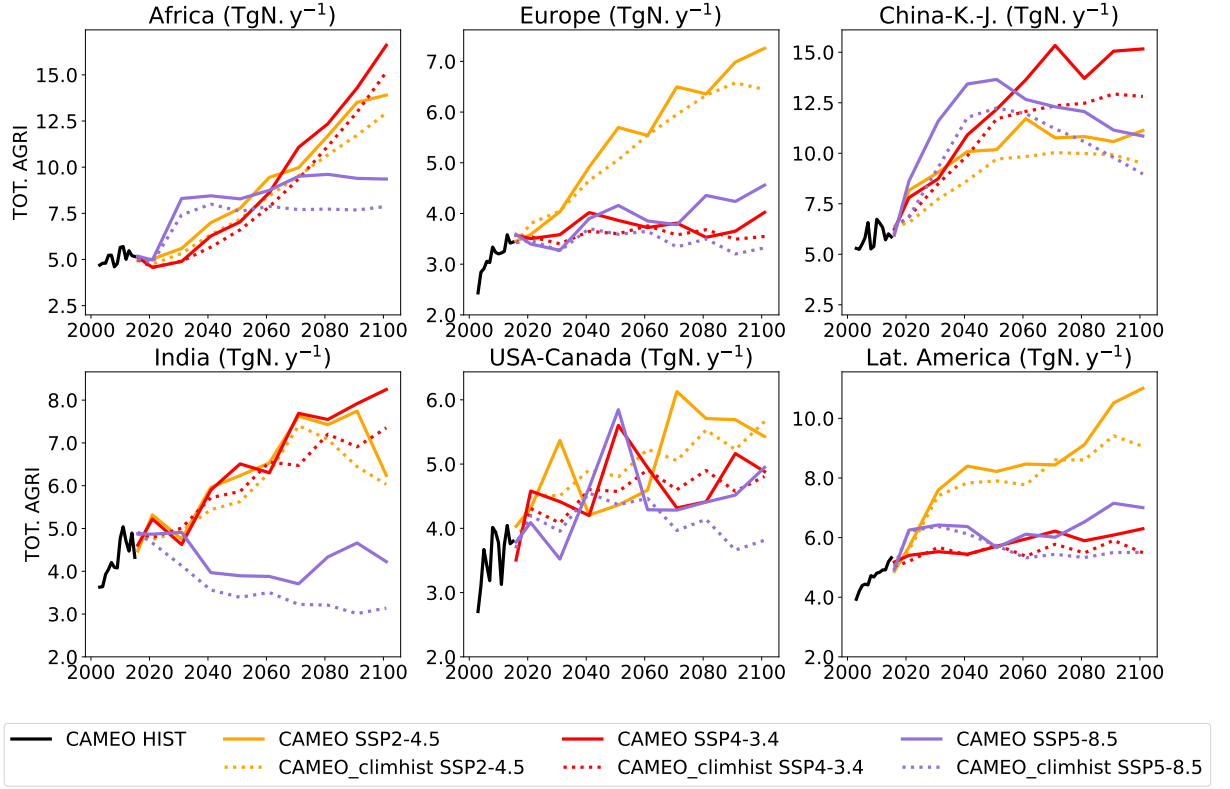|	CAMEO	CAMEO$_{\text{ClimHIST}}$	IAMs
HIST (present-day)	34	34	36
SSP2-4.5 (future)	70	64	38
SSP4-3.4 (future)	68	63	66
SSP5-8.5 (future)	50	39	53

Figure 5. Evolution of the global agricultural NH$_3$ emissions for the considered SSPs from CAMEO under future climate (solid lines) and under a historical climate (dotted lines) in TgN.yr^{-1}.

3.3 Global and regional agricultural emissions in 2100

Figure 6 displays the distributions of the absolute changes in the future emissions (2091-2100) compared to the historical period (2005-2014 here) over the biggest hotspot regions. While China, India, and Europe highlight the most important NH$_3$ fluxes ($>$ 4 gN.m^{-2}.yr^{-1}) during the historical period (2014), the most important changes (reaching more than 4 gN.m^{-2}.yr^{-1}) are located in the Maghreb and South Africa under SSP4-3.4 and over the southeastern US under SSP2-4.5. Northern India and China also highlight important increases under both SSP2-4.5 and SSP4-3.4 scenarios. Despite a global increase under all the SSPs, there are regions where emissions slightly decrease, especially under SSP5-8.5 in India, Argentina, and Equatorial Africa, where negative anomalies can reach 2 gN.m^{-2}.yr^{-1}. Because of the spatial heterogeneity in the 2091-2100 simulated emissions over Africa and Asia, both regions will be further analyzed.

The evolution of agricultural emissions is contrasted over the African continent with three specific regions: Northern Maghreb, the Sahelian savanna, and Southern Africa. Northern Maghreb is characterized by a substantial increase in the emissions under SSP4-3.4 which can be directly attributed to the large increase in the mineral fertilizer use ($+10$ gN.m^{-2}.yr^{-1}, Figure S7 in the Supplementary Material). In addition to the mineral fertilizer, we observe an extension of cropland areas in the coastal region of Maghreb (at
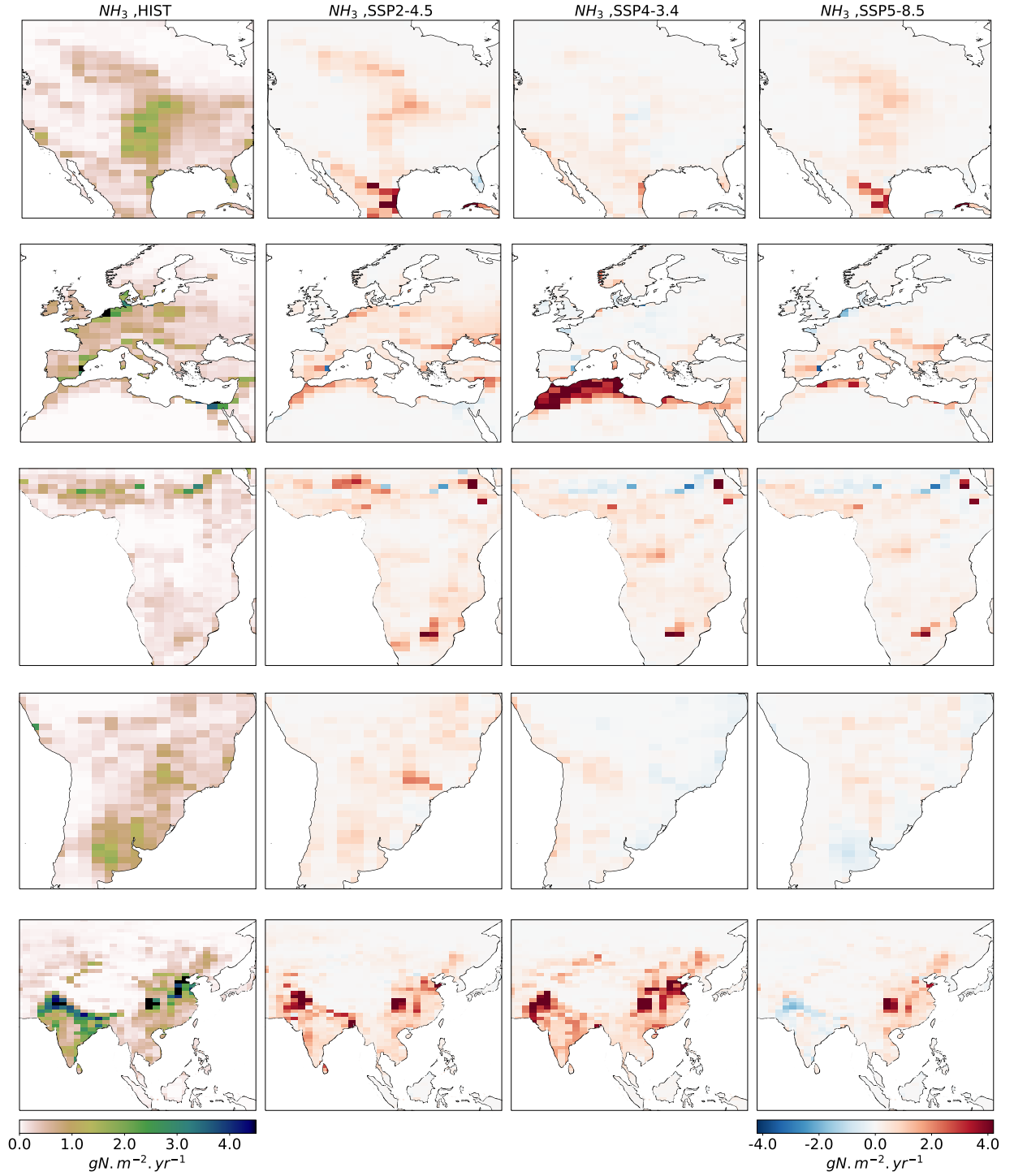
Figure 6. Agricultural emissions in the historical period (2005-2014, first column) and absolute differences between future (2091-2100) and historical emissions under the three SSPs (second, third and last columns) simulated by CAMEO under future climate. Units are in gN.m^{-2}.yr^{-1}

the expense of grassland) and also towards the South, where no cropland area is present in the historical period (Figure S9 in the Supplementary Material).

Regarding the Southern African pattern, a similar increase in agricultural emissions is encountered under all the SSPs in 2100. This region is associated with an enhancement of the produced and applied manure where the absolute difference between the historical and future periods can reach 10 $gN.m^{-2}.yr^{-1}$ while the present-day manure produced does not exceed 1 $gN.m^{-2}.yr^{-1}$. The important enhancement of the NPP of grass in this region (> 0.4 $kgC.m^{-2}.yr^{-1}$) suggests that the future ruminant population can be easily maintained and therefore might be the location where the regional livestock increase has been allocated in our methodology (Figure S9 in the Supplementary Material).

In Asia, the change in emissions is also contrasted spatially; India and China differ significantly, especially under the SSP5-8.5. While emissions in Northern India will slow down (-1 $gN.m^{-2}.yr^{-1}$), in central China, we observe an increase reaching more than 4 $gN.m^{-2}.yr^{-1}$. The evolution of the agricultural emissions under the SSP5-8.5 over India (Figure S8 in the Supplementary Material) can be attributed to the decrease in the N input (both fertilizer and manure). On the contrary, under SSP4-3.4, the fertilizer rate in Asia highly increases in 2100 compared to the historical period, especially in China (≥ 8 $gN.m^{-2}.yr^{-1}$). Under the SSP5-8.5 in central China, only manure N input contributes to the enhancement of the emission since almost no change in the use of synthetic fertilizer is observed (Figure S8 in the Supplementary Material). The evolution of the emissions by the IAMs in the context of CMIP6 highlights very different patterns than what is described in CAMEO (Figure S10 in the Supplementary Material). The most important changes (≥ 2 $gN.m^{-2}.yr^{-1}$) are concentrated over Africa under SSP4-3.4 and SSP5-8.5.

4 Discussion and conclusions

In this paper, we investigated future NH_3 emissions using the process-based model CAMEO and taking into account future livestock densities. Future gridded livestock densities are constructed for 3 SSPs taking into account accurate biomass availability and future regional livestock productions. This new dataset constitutes a major input for future global emission projections. We estimated a future increase of NH_3 emissions ranging from 50 to 70 $TgN.yr^{-1}$ in 2100 depending on the scenario considered. The manure produced most likely contributes to slow down the emissions as a result of regional livestock production trends and of local feeding resource limitations. Contrary to manure production, the synthetic fertilizer rate is likely to increase substantially in most regions (especially under the SSP2-4.5 and SSP4-3.4). These trends are in agreement with the lack of future regulation regarding the food sector. Our approach shows its ability to simulate future global emissions in response to future changes in agricultural activities and land use but also climate change. Indeed, [CO_2], temperature and precipitations have both direct and indirect effects on the NH_3 emissions in CAMEO. These three factors impact the growth of the vegetation which modifies its capacity in absorbing the nutrient and thus the nitrogen available for volatilization. In addition, temperature and precipitation are involved in the physical-chemical reactions at the surface-atmosphere interface, leading to the volatilization of ammonia.

A limitation in future emissions is reflected by the lack of synthetic N input over grasslands in the CMIP6 framework. In reality, the synthetic fertilization of grassland areas is non-negligible and might play a role in the future, especially with the expected land use changes and the impact on ruminant activities. In CAMEO, grasslands contribute to 30% of the total agricultural emissions in 2100 under the SSP5-8.5, mainly from the manure produced by ruminants whose population is directly regulated by their productivity. In addition, the IAMs framework involves a harmonization of the emissions

among all the SSPs, meaning that the historical point also defines the trajectory of the emissions, which can mask the evolution, over the early decades of the 21st century, of agricultural input, for example.

Compared to IAM-based approach, CAMEO has a more realistic representation of NH_3 emissions, but strong assumptions are used and might induce some biases. For instance, our method to estimate future livestock population does not take into account the change in the productivity of the grassland which might be affected by an enhanced fertilization rate coming from mineral fertilizer use but also atmospheric nitrogen depositions and atmospheric CO_2 concentration. In the future, human diet shifts might impact the distributions of the livestock categories (i.e ruminants, pigs, poultry). However, because no data is currently available regarding the future evolution of the different livestock types, we assume no change in our future estimates. This assumption leads to a similar constraint applied in the ruminant and non-ruminant populations when the grassland is locally limited, while non-ruminants mainly rely on crops.

Many studies are based on livestock densities for the present day to estimate future manure production or N and methane emissions (B. Zhang et al., 2017; Vira et al., 2019; L. Zhang et al., 2021). Since no other gridded livestock distributions have been projected for future decades, our approach constitutes a new potential helpful input for other future studies requiring global livestock population densities.

Data Availability Statement

The simulated data used for figure plotting in this paper can be accessed from the Zenodo repository: https://zenodo.org/records/10100435.

References

Barona, E., Ramankutty, N., Hyman, G., & Coomes, O. T. (2010, April). The role of pasture and soybean in deforestation of the Brazilian Amazon. *Environmental Research Letters*, *5*(2), 024002. Retrieved 2022-08-03, from `https://iopscience.iop.org/article/10.1088/1748-9326/5/2/024002` doi: 10.1088/1748-9326/5/2/024002

Beaudor, M., Vuichard, N., Lathière, J., Evangeliou, N., Van Damme, M., Clarisse, L., & Hauglustaine, D. (2023, February). Global agricultural ammonia emissions simulated with the ORCHIDEE land surface model. *Geoscientific Model Development*, *16*(3), 1053–1081. Retrieved 2023-05-12, from `https://gmd.copernicus.org/articles/16/1053/2023/` (Publisher: Copernicus GmbH) doi: 10.5194/gmd-16-1053-2023

Bian, H., Chin, M., Hauglustaine, D. A., Schulz, M., Myhre, G., Bauer, S. E., ... Tsyro, S. G. (2017, November). Investigation of global particulate nitrate from the AeroCom phase III experiment. *Atmospheric Chemistry and Physics*, *17*(21), 12911–12940. Retrieved 2022-10-27, from `https://acp.copernicus.org/articles/17/12911/2017/` doi: 10.5194/acp-17-12911-2017

Boucher, O., Denvil, S., Levavasseur, G., Cozic, A., Caubel, A., Foujols, M.-A., ... Lurton, T. (2019). *IPSL IPSL-CM6A-LR model output prepared for CMIP6 ScenarioMIP ssp245.* Retrieved 2022-09-07, from `https://doi.org/`

10.22033/ESGF/CMIP6.5264 (Publisher: Earth System Grid Federation) doi: 10.22033/ESGF/CMIP6.5264

Boucher, O., Servonnat, J., Albright, A. L., Aumont, O., Balkanski, Y., Bastrikov, V., . . . Vuichard, N. (2020). Presentation and Evaluation of the IPSL-CM6A-LR Climate Model. *Journal of Advances in Modeling Earth Systems*, *12*(7), e2019MS002010. Retrieved 2022-03-11, from https://onlinelibrary.wiley.com/doi/abs/10.1029/2019MS002010 (_eprint: https://onlinelibrary.wiley.com/doi/pdf/10.1029/2019MS002010) doi: 10.1029/2019MS002010

Calvin, K., Bond-Lamberty, B., Clarke, L., Edmonds, J., Eom, J., Hartin, C., . . . Wise, M. (2017, January). The SSP4: A world of deepening inequality. *Global Environmental Change*, *42*, 284–296. Retrieved 2023-11-18, from https://linkinghub.elsevier.com/retrieve/pii/S095937801630084X doi: 10.1016/j.gloenvcha.2016.06.010

Collins, W. J., Lamarque, J.-F., Schulz, M., Boucher, O., Eyring, V., Hegglin, M. I., . . . Smith, S. J. (2017, February). AerChemMIP: quantifying the effects of chemistry and aerosols in CMIP6. *Geoscientific Model Development*, *10*(2), 585–607. Retrieved 2023-06-18, from https://gmd.copernicus.org/articles/10/585/2017/gmd-10-585-2017.html (Publisher: Copernicus GmbH) doi: 10.5194/gmd-10-585-2017

Evangeliou, N., Balkanski, Y., Eckhardt, S., Cozic, A., Damme, V., Coheur, P.-F., . . . Hauglustaine, D. (2020). 1 10–year satellite–constrained fluxes of ammonia improve 2 performance of chemistry transport models. , 41.

Fricko, O., Havlik, P., Rogelj, J., Klimont, Z., Gusti, M., Johnson, N., . . . Riahi, K. (2017, January). The marker quantification of the Shared Socioeconomic Pathway 2: A middle-of-the-road scenario for the 21st century. *Global Environmental Change*, *42*, 251–267. Retrieved 2022-09-05, from https://linkinghub.elsevier.com/retrieve/pii/S0959378016300784 doi: 10.1016/j.gloenvcha.2016.06.004

Gidden, M. J., Fujimori, S., van den Berg, M., Klein, D., Smith, S. J., van Vuuren, D. P., & Riahi, K. (2018, July). A methodology and implementation of automated emissions harmonization for use in Integrated Assessment Models. *Environmental Modelling & Software*, *105*, 187–200. Retrieved 2022-10-03, from https://www.sciencedirect.com/science/article/pii/S1364815217307867 doi: 10.1016/j.envsoft.2018.04.002

Hauglustaine, D. A., Balkanski, Y., & Schulz, M. (2014, October). A global model simulation of present and future nitrate aerosols and their direct radiative forcing of climate. *Atmospheric Chemistry and Physics*, *14*(20), 11031–11063. Retrieved 2020-08-07, from https://acp.copernicus.org/articles/14/11031/2014/ doi: 10.5194/acp-14-11031-2014

Hegglin, M., Kinnison, D., & Lamarque, J.-F. (2016). *CCMI nitrogen surface fluxes in support of CMIP6 - version 2.0.* Retrieved 2022-11-05, from https://doi.org/10.22033/ESGF/input4MIPs.1125 (Publisher: Earth System Grid Federation) doi: 10.22033/ESGF/input4MIPs.1125

Hegglin, M., Kinnison, D., & Plummer, D. (n.d.). *Historical and future ozone database (1850-2100) in support of CMIP6, in preparation.* Retrieved 2023-07-03, from https://blogs.reading.ac.uk/ccmi/forcing-databases-in-support-of-cmip6/

Herrero, M., Thornton, P. K., Gerber, P., & Reid, R. S. (2009, December). Livestock, livelihoods and the environment: understanding the trade-offs. *Current Opinion in Environmental Sustainability*, *1*(2), 111–120. Retrieved 2022-08-03, from https://www.sciencedirect.com/science/article/pii/S1877343509000335 doi: 10.1016/j.cosust.2009.10.003

Hoesly, R. M., Smith, S. J., Feng, L., Klimont, Z., Janssens-Maenhout, G., Pitkanen, T., . . . Zhang, Q. (2018, January). Historical (1750–2014) anthropogenic

emissions of reactive gases and aerosols from the Community Emissions Data System (CEDS). *Geoscientific Model Development*, *11*(1), 369–408. Retrieved 2021-08-26, from `https://gmd.copernicus.org/articles/11/369/2018/` (Publisher: Copernicus GmbH) doi: 10.5194/gmd-11-369-2018

Hurtt, G. C., Chini, L., Sahajpal, R., Frolking, S., Bodirsky, B. L., Calvin, K., . . . Zhang, X. (2020, November). Harmonization of global land use change and management for the period 850–2100 (LUH2) for CMIP6. *Geoscientific Model Development*, *13*(11), 5425–5464. Retrieved 2021-11-15, from `https://gmd.copernicus.org/articles/13/5425/2020/` doi: 10.5194/gmd-13-5425-2020

Janssens-Maenhout, G. (2011, December). EDGARv4.2 Emission Maps. Retrieved 2022-09-06, from `http://data.europa.eu/89h/jrc-edgar-emissionmapsv42` (Publisher: European Commission, Joint Research Centre (JRC))

Kriegler, E., Bauer, N., Popp, A., Humpenöder, F., Leimbach, M., Strefler, J., . . . Edenhofer, O. (2017, January). Fossil-fueled development (SSP5): An energy and resource intensive scenario for the 21st century. *Global Environmental Change*, *42*, 297–315. Retrieved 2022-09-05, from `https://www.sciencedirect.com/science/article/pii/S0959378016300711` doi: 10.1016/j.gloenvcha.2016.05.015

Krinner, G., Viovy, N., Noblet-Ducoudré, N. d., Ogée, J., Polcher, J., Friedlingstein, P., . . . Prentice, I. C. (2005). A dynamic global vegetation model for studies of the coupled atmosphere-biosphere system. *Global Biogeochemical Cycles*, *19*(1). Retrieved 2021-06-28, from `https://agupubs.onlinelibrary.wiley.com/doi/abs/10.1029/2003GB002199` doi: 10.1029/2003GB002199

Lurton, T., Balkanski, Y., Bastrikov, V., Bekki, S., Bopp, L., Braconnot, P., . . . Boucher, O. (2020). Implementation of the CMIP6 Forcing Data in the IPSL-CM6A-LR Model. *Journal of Advances in Modeling Earth Systems*, *12*(4), e2019MS001940. Retrieved 2022-03-11, from `https://onlinelibrary.wiley.com/doi/abs/10.1029/2019MS001940` (_eprint: https://onlinelibrary.wiley.com/doi/pdf/10.1029/2019MS001940) doi: 10.1029/2019MS001940

O'Neill, B. C., Tebaldi, C., van Vuuren, D. P., Eyring, V., Friedlingstein, P., Hurtt, G., . . . Sanderson, B. M. (2016, September). The Scenario Model Intercomparison Project (ScenarioMIP) for CMIP6. *Geoscientific Model Development*, *9*(9), 3461–3482. Retrieved 2022-09-06, from `https://gmd.copernicus.org/articles/9/3461/2016/` (Publisher: Copernicus GmbH) doi: 10.5194/gmd-9-3461-2016

Pai, S. J., Heald, C. L., & Murphy, J. G. (2021, July). Exploring the Global Importance of Atmospheric Ammonia Oxidation. *ACS Earth and Space Chemistry*, *5*(7), 1674–1685. Retrieved 2021-09-30, from `https://pubs.acs.org/doi/10.1021/acsearthspacechem.1c00021` doi: 10.1021/acsearthspacechem.1c00021

Paulot, F., Ginoux, P., Cooke, W. F., Donner, L. J., Fan, S., Lin, M.-Y., . . . Horowitz, L. W. (2016, February). Sensitivity of nitrate aerosols to ammonia emissions and to nitrate chemistry: implications for present and future nitrate optical depth. *Atmospheric Chemistry and Physics*, *16*(3), 1459–1477. Retrieved 2022-06-06, from `https://acp.copernicus.org/articles/16/1459/2016/` doi: 10.5194/acp-16-1459-2016

Paustian, K., ravindranath, n., & Van Amstel, A. (2006). *IPCC Guidelines for National Greenhouse Gas Inventories. Volume 4 Agriculture, forestry and other land use.*

Popp, A., Calvin, K., Fujimori, S., Havlik, P., Humpenöder, F., Stehfest, E., . . . Vuuren, D. P. v. (2017, January). Land-use futures in the shared socio-economic pathways. *Global Environmental Change*, *42*, 331–345. Retrieved 2023-11-18, from `https://www.sciencedirect.com/science/article/pii/`

S0959378016303399 doi: 10.1016/j.gloenvcha.2016.10.002

Rao, S., Klimont, Z., Smith, S. J., Van Dingenen, R., Dentener, F., Bouwman, L., ... Tavoni, M. (2017, January). Future air pollution in the Shared Socio-economic Pathways. *Global Environmental Change*, *42*, 346–358. Retrieved 2022-09-05, from `https://linkinghub.elsevier.com/retrieve/pii/S0959378016300723` doi: 10.1016/j.gloenvcha.2016.05.012

Reid, R., Galvin, K., & Kruska, R. (2008, January). Global Significance of Extensive Grazing Lands and Pastoral Societies: An Introduction. In *Fragmentation in Semi-Arid and Arid Landscapes: Consequences for Human and Natural Systems* (pp. 1–24). (Journal Abbreviation: Fragmentation in Semi-Arid and Arid Landscapes: Consequences for Human and Natural Systems) doi: 10.1007/978-1-4020-4906-4_1

Riahi, K., van Vuuren, D. P., Kriegler, E., Edmonds, J., O'Neill, B. C., Fujimori, S., ... Tavoni, M. (2017, January). The Shared Socioeconomic Pathways and their energy, land use, and greenhouse gas emissions implications: An overview. *Global Environmental Change*, *42*, 153–168. Retrieved 2022-02-11, from `https://linkinghub.elsevier.com/retrieve/pii/S0959378016300681` doi: 10.1016/j.gloenvcha.2016.05.009

Robinson, T. P., Wint, G. R. W., Conchedda, G., Van Boeckel, T. P., Ercoli, V., Palamara, E., ... Gilbert, M. (2014, May). Mapping the Global Distribution of Livestock. *PLoS ONE*, *9*(5), e96084. Retrieved 2020-02-14, from `https://dx.plos.org/10.1371/journal.pone.0096084` doi: 10.1371/journal.pone.0096084

van Marle, M. J. E., Kloster, S., Magi, B. I., Marlon, J. R., Daniau, A.-L., Field, R. D., ... van der Werf, G. R. (2017, September). Historic global biomass burning emissions for CMIP6 (BB4CMIP) based on merging satellite observations with proxies and fire models (1750–2015). *Geoscientific Model Development*, *10*(9), 3329–3357. Retrieved 2021-11-29, from `https://gmd.copernicus.org/articles/10/3329/2017/` (Publisher: Copernicus GmbH) doi: 10.5194/gmd-10-3329-2017

Vira, J., Hess, P., Melkonian, J., & Wieder, W. R. (2019, August). An improved mechanistic model for ammonia volatilization in Earth system models: Flow of Agricultural Nitrogen, version 2 (FANv2). *Geoscientific Model Development Discussions*, 1–49. Retrieved 2019-11-13, from `https://www.geosci-model-dev-discuss.net/gmd-2019-233/` doi: 10.5194/gmd-2019-233

Vuichard, N., Messina, P., Luyssaert, S., Guenet, B., Zaehle, S., Ghattas, J., ... Peylin, P. (2019, November). Accounting for carbon and nitrogen interactions in the global terrestrial ecosystem model ORCHIDEE (trunk version, rev 4999): multi-scale evaluation of gross primary production. *Geoscientific Model Development*, *12*(11), 4751–4779. Retrieved 2021-10-08, from `https://gmd.copernicus.org/articles/12/4751/2019/` (Publisher: Copernicus GmbH) doi: 10.5194/gmd-12-4751-2019

Zhang, B., Tian, H., Lu, C., Dangal, S. R. S., Yang, J., & Pan, S. (2017, September). Global manure nitrogen production and application in cropland during 1860–2014: a 5 arcmin gridded global dataset for Earth system modeling. *Earth System Science Data*, *9*(2), 667–678. Retrieved 2020-02-14, from `https://www.earth-syst-sci-data.net/9/667/2017/` doi: 10.5194/essd-9-667-2017

Zhang, L., Tian, H., Shi, H., Pan, S., Qin, X., Pan, N., & Dangal, S. R. (2021, January). Methane emissions from livestock in East Asia during 19612019. *Ecosystem Health and Sustainability*, *7*(1), 1918024. Retrieved 2022-10-05, from `https://doi.org/10.1080/20964129.2021.1918024` (Publisher: Taylor & Francis _eprint: https://doi.org/10.1080/20964129.2021.1918024) doi: 10.1080/20964129.2021.1918024